Selective Formation of Zigzag Edges in Graphene Cracks

Miho Fujihara,[†] Ryosuke Inoue,[‡] Rei Kurita,[‡] Toshiyuki Taniuchi,[§] Yoshihito Motoyui,[§] Shik Shin,[§] Fumio Komori,[§] Yutaka Maniwa,[‡] Hisanori Shinohara,[*,†] and Yasumitsu Miyata[*,‡,⊥]

[†]Department of Chemistry, Nagoya University and Institute for Advanced Research, Nagoya 464-8602, Japan, [‡]Department of Physics, Tokyo Metropolitan University, Hachioji, Tokyo 192-0397, Japan, [§]Institute for Solid State Physics, The University of Tokyo, Kashiwa, Chiba 277-8581, Japan, and [⊥]JST-PRESTO, Kawaguchi, Saitama 332-0012, Japan

ABSTRACT We report the thermally induced unconventional cracking of graphene to generate zigzag edges. This crystallography-selective cracking was observed for as-grown graphene films immediately following the cooling process subsequent to chemical vapor deposition (CVD) on Cu foil. Results from Raman spectroscopy show that the crack-derived edges have smoother zigzag edges than the chemically formed grain edges of CVD graphene. Using these cracks as nanogaps, we were also able to demonstrate the carrier tuning of graphene through the electric field effect. Statistical analysis of visual observations indicated that the crack formation results from uniaxial tension imparted by the Cu substrates together with the stress concentration at notches in the polycrystalline graphene films. On the basis of simulation results using a simplified thermal shrinkage model, we propose that the cooling-induced tension is derived from the transient lattice expansion of narrow Cu grains imparted by the thermal shrinkage of adjacent Cu grains.

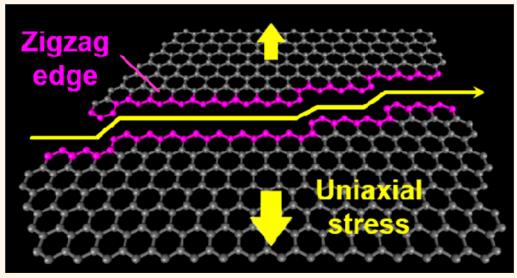

KEYWORDS: graphene · cracking · cleavage · zigzag edge · nanogaps

Graphene, a one-atom-thick carbon sheet with a honeycomb structure, is a representative two-dimensional material with excellent electronic and mechanical properties.[1−5] One of the unique aspects of graphene is its edge structure, which is generally classified into zigzag or armchair edges. These graphene edges have attracted much attention due to their unique structure-dependent electronic and magnetic properties, as well as their effects on bulk carrier transport properties. In initial studies, these properties were primarily studied theoretically because they could be modeled by simple systems.[6,7] Recent progress in experimental studies has also revealed the local stability and electronic properties of graphene edges through the use of scanning probe microscopy (SPM) and high-resolution transmission electron microscopy (HR-TEM).[8−10] Since previous studies were limited to the analysis of local properties on the nanometer or atomic scale, the macroscopic electric and magnetic properties of graphene edges are still unclear. This primarily stems from the difficulty in preparing high-quality graphene edges. To allow for further investigation and application of graphene edges, it is, therefore, highly desirable to develop a sophisticated method for the preparation of smooth, clean edges with the desired structure.

To date, the preparation and structural control of graphene edges has been conducted using various methods, including chemical etching,[11−15] mechanical cleavage,[5,16−18] and others.[8,10,19−21] For example, it is known that chemical etching with hydrogen enables the preferential formation of zigzag edges. However, SPM studies suggest that there is still atomic-level roughness along the chemically formed edges.[11] In contrast, in a previous study, in-plane tearing of suspended graphene generated atomically smooth edges composed of both zigzag and armchair structures.[16] In this case, the tearing of the graphene was initiated by electron beam irradiation during TEM observation, and cracks propagated with the assistance of inhomogeneous internal tension probably generated during transfer of the graphene onto a TEM grid. Considering the atomically smooth and clean edges observed, it is a fascinating challenge to selectively prepare zigzag or armchair edges by

* Address correspondence to ymiyata@tmu.ac.jp, noris@nagoya-u.jp.

Received for review May 21, 2015 and accepted August 19, 2015.

Published online August 19, 2015
10.1021/acsnano.5b03079

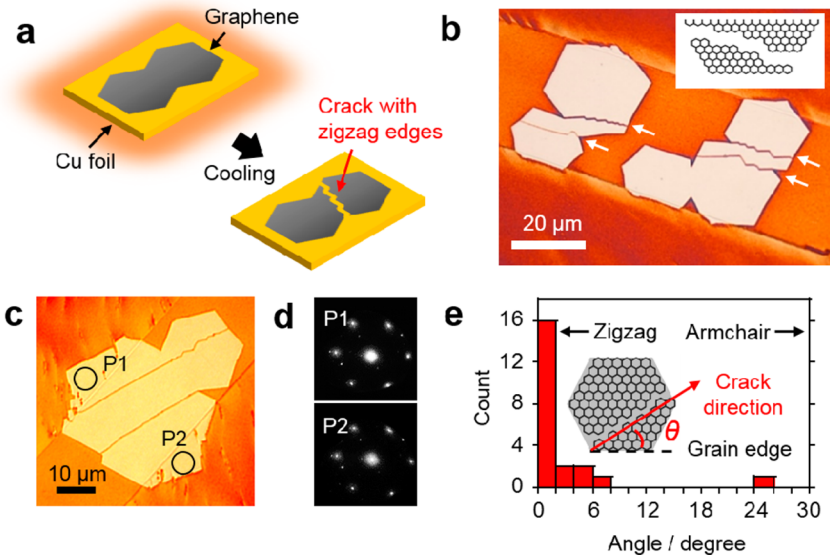

Figure 1. (a) Schematic illustration of crack formation in the graphene film during the postgrowth cooling process. (b,c) Optical images of graphene films with cracks on oxidized Cu foil. White arrows indicate cracks connected with V-shaped notches in the films. (d) Low-energy electron diffraction patterns of the graphene taken within the area indicated by solid circles P1 and P2 in (c). (e) Distribution of the crack directions relative to the grain edge. In the present study, we counted all adequately straight cracks more than 5 μm in length. Crack angles of 0 and 30° correspond to the zigzag and armchair directions, respectively.

mechanical cleavage. It is worthwhile to note that there are several theoretical simulations of tearing graphene. In some cases, the calculation results show the preferential formation of armchair or zigzag edges depending on various factors such as the direction of the force.[22−24] Among these reports, a molecular dynamics (MD) simulation study predicts that applying in-plane tensile stress to prenotched graphene leads to the preferential formation of cracks with zigzag edges.[22,24] In the present study, we found that a similar situation can be reproduced in an actual experimental system.

Herein, we report that cracks in graphene can selectively propagate along a zigzag edge orientation under uniaxial tension that is applied to graphene on copper foil during the cooling process following chemical vapor deposition (CVD) (Figure 1a). Results from Raman spectroscopy indicate that this produces smoother zigzag edges than the chemically formed grain edges of CVD graphene. We have also shown the modulation of carrier density in graphene as a result of applying an electric field to such cracks. Statistical optical microscope observations indicate that the cracking is caused by a combination of uniaxial tension and the stress concentration at the notches on the polycrystalline graphene films. On the basis of the results of numerical simulations of a simplified thermal shrinkage model, we propose that the uniaxial tension originates from the transient lattice expansion of narrow Cu grains induced by thermal shrinking of adjacent Cu grains.

RESULTS AND DISCUSSION

Figure 1b shows an optical image of polycrystalline graphene films exhibiting cracks on Cu foil. To enhance the contrast of the cracks, the bare Cu was oxidized by heating for 5−10 min at 160 °C, as described in a previous study.[25] We note that these cracks can be observed without the thermal oxidation of Cu using scanning electron microscopy (SEM) (Figure S1) and that the oxidation process does not affect the crack formation. It is also noteworthy that each crack turns around at 60° angles several times (we call this behavior the "60° turning rule") and that the crack directions are nearly parallel to the edges of the hexagonal graphene grains. As reported previously, it is well-known that the grain edges are parallel to the zigzag edges.[26] This was also confirmed in the present study based on the relationship between the crack direction in Figure 1c and rotation-calibrated low-energy electron diffraction (LEED) patterns (Figure 1d). We found that the directions of over 90% of the graphene cracks were almost parallel (within 6°) to the zigzag edges, as shown in Figure 1e. This anisotropic crack propagation indicates the selective formation of zigzag edges during the cracking, as illustrated in the inset of Figure 1b.

We found that the so-called "60° turning rule" was violated when cracks propagate across the grain boundaries in polycrystalline graphene films consisting of grains with different crystal orientations. Figure 2a shows an SEM image of a crack in a polycrystalline graphene film. Interestingly, the crack profiles change from zigzag (right region) to straight (left region). Almost the same change in the crack profile is observed in the optical image of another graphene film presented in Figure 2b. This variation is found to occur near the grain boundary, as illustrated in Figure 2c and the inset of Figure 2a. The presence of a grain boundary

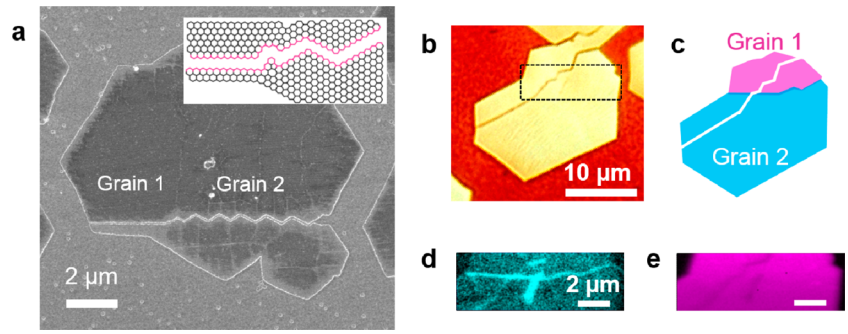

Figure 2. (a) SEM image of a cracked polycrystalline graphene film on Cu foil. Inset: Simplified structure model of the film near the point of variation in the crack profile. Note that the model is tentatively described to be hundreds of times smaller than that of the actual graphene grain in the SEM image and to have smooth edges and narrow crack width. (b) Optical image of a cracked polycrystalline graphene film on oxidized Cu foil. (c) Schematic illustration representing the grain boundary of the graphene film in (b). The pink and blue regions correspond to graphene grains with different crystal orientations, while the white line indicates the crack. (d) D-band and (e) 2D-band Raman intensity maps of the graphene film within the rectangular area outlined in (b). Raman maps were acquired after transferring the graphene from the Cu foil to a SiO_2/Si substrate. The D-band intensity of the crack is relatively weak because of the misalignment of the optical polarization of the excitation laser.

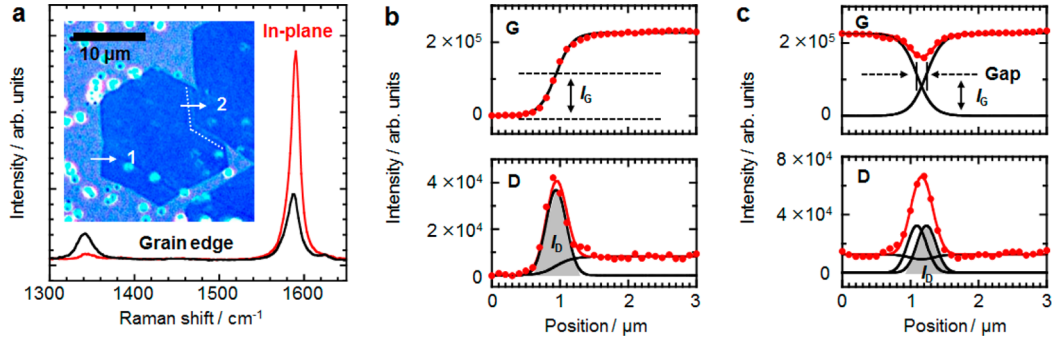

Figure 3. (a) Raman spectra of graphene in the grain (red) and the edge located at the grain (black). Inset: optical image of graphene grains transferred onto a SiO_2/Si substrate. G-band (top panel) and D-band (bottom panel) intensity profiles along (b) the arrow labeled 1 crossing the grain edge in (a) and (c) the arrow labeled 2 crossing the crack-derived edges in (a). Raman spectra were acquired at 100 nm intervals, and each intensity value was obtained from the D-band and G-band peak areas.

is confirmed from the increase in the D-band intensity in the Raman intensity map (Figure 2d) and spectrum (Figure S2), as was also observed in a previous study.[27] Because the graphene grain is a continuous sheet across the grain boundary, along the boundary, the Cu surface is free from oxidation unlike the bare Cu in the crack in Figure 2b, and no reduction of the 2D-band intensity is observed in Figure 2e. These situations support the presence of a grain boundary, as illustrated in Figure 2c. For this reason, we find that a change in the crack profiles occurs in the vicinity of the grain boundaries, and that crystallographic orientation of graphene plays a significant role in the graphene cracking. In other words, the present result indicates that the grain boundaries are sufficiently robust against cracking, as observed in nanoindentation test.[28] We note that the present cracking starts from the notches of graphene grains as described later. This may be one of the possible reasons why we cannot see apparent grain boundary cracking as predicted by previous theoretical works.[29,30]

In the following section, we compare the quality of the crack-derived zigzag edges with that of the edges formed around graphene grains (that is, the grain edges). In the present study, the crystallinity of the zigzag edges was investigated using Raman spectroscopy because the D-band intensity is known to increase with an increase in the concentration of armchair edges.[17,31,32] The ratio of the D-band and G-band intensities at the edges was estimated from the fitting of the intensity profile across the edges to allow for reproducible and quantitative comparisons (Figure 3). We note that the crack edges can be distinguished from the grains boundaries through atomic force microscopy (AFM) observations (Figure S3) and the contrast of the optical image on Cu foil as presented above. This fitting-based analysis was able to separate the contribution of the finite D-band intensity originating within the in-plane area of the graphene, as shown in Figure 3a, from the edge D-band intensity. Furthermore, we were able to suppress the effects of variations in the position on the Raman intensities at the edges. As shown in Figures 3b,c and S4, a positional shift of just 100 nm is sufficient to affect the Raman intensities around the edges.

During this analysis, the G-band intensity profiles at the grain edge and the crack edges could be fit using single and double sigmoid curves, respectively (top panel in Figure 3b,c). Because the position having half the maximum intensity, I_G, corresponds to the edge,

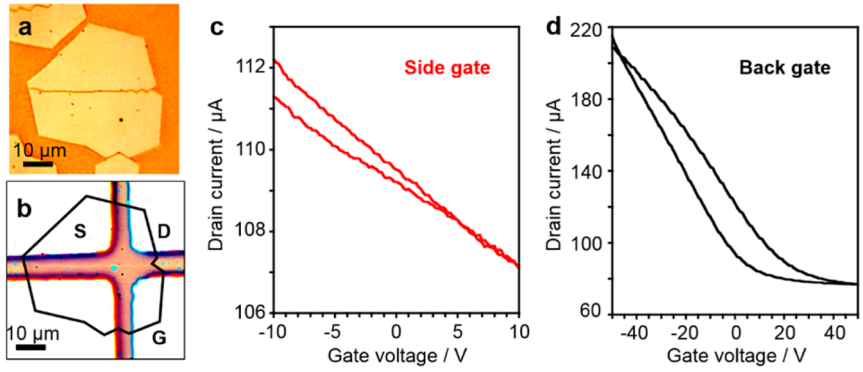

Figure 4. Optical images of graphene (a) on Cu foil and (b) on a SiO_2/Si substrate (SiO_2 layer thickness = 285 nm) with electrodes. White colored areas in (b) are Au/Cr electrodes. I_D-V_{GS} characteristics of (c) the side-gated FET and (d) the back-gated FET. The source−drain voltage was held constant at $V_{DS} = -0.01$ V.

I_G was taken as equal to the G-band intensity at the edges. The D-band intensity profiles could be fit using the sum of a single (double) sigmoid curve and a single (double) Gaussian curve for grain (crack) edges, as shown in the bottom panels in Figure 3b,c. The normalized area of the Gaussian curves was taken as equal to the D band intensity, I_D, at the edge to suppress the scattering of data due to the fluctuation of spatial resolution in our optical system. It is worth noting that the fitting curves indicate that the crack gap in Figure 3a is approximately 140 nm. This value is in good agreement with the gap width of 100 nm estimated from AFM observations (Figure S3). In this manner, we determined the I_D/I_G ratios of 16 crack edges and 17 grain edges, and the results are summarized in Figure S5. The averages (standard deviation) of I_D/I_G ratios are 0.048 (0.007) and 0.062 (0.009) for the crack and grain edges, respectively. The average of the crack edges is smaller than that of the grain edge, which suggests that the cracks have fewer armchair edges than the grain edges. In other words, these results indicate that the crack-derived edges could have smoother zigzag structures than the chemically formed grain edges.

In addition to smooth edges, the cracking can easily produce two parallel edges in the graphene grains with a gap of approximately 100 nm. To demonstrate a potential application of graphene cracks we fabricated side-gated monolayer field-effect transistors (FETs) using graphene. Because current cannot flow across these cracks, using one side of the graphene as a side-gate electrode enables the modulation of the carrier density in the other side. As a means of assessing electrical properties, a graphene film with a single crack on Cu foil was transferred to a SiO_2/Si substrate, following which three electrodes were deposited on the graphene grains using a shadow mask (Figure 4a,b). We note that there are no noticeable changes in the size and width of cracks after the transfer. Figure 4c shows the I_D-V_{GS} characteristics of the FET obtained from side-gate measurements. The source−drain current is seen to decrease with increasing gate voltage and could be modulated by a factor of approximately 4% by varying the side-gate voltage from −10 to +10 V. The degree of modulation in this device was lower than that obtained from a back-gate device (approximately 30% over the back-gate voltage range from −10 to +10 V, Figure 4d). These data suggest the spatially different electric field effects between side- and back-gate devices that may possibly provide a means of controlling the carrier density in graphene edges.

Finally, we focused our attention on the formation conditions and the mechanisms by which the observed anisotropic cracks were generated in the graphene. The present cracks were found to have three primary features. First, the majority of the cracks proceeded from V-shaped notches formed at the grain boundary of the graphene through the fusion of two hexagonal-shaped grains during CVD growth (Figures 1b,c and 5a). Even when working at a micrometer-scale spatial resolution, statistical analysis of specimen observations was able to determine that at least 80% of the cracks (87/112) were connected to the notches. These notches allow the graphene to tear easily as the result of stress concentrations, in accordance with prior simulations.[22,24] Second, the cracks were primarily seen in graphene grains grown on Cu grains in the form of narrow strips having widths of several tens of micrometers (Figures 1b,c and 5a). Electron backscatter diffraction (EBSD) analysis (Figure S6) and LEED patterns (Figure S7) demonstrated that these strip-shaped grains correspond to a Cu(100) face surrounded by a Cu(111) face. Almost no cracks were observed on the majority of the graphene grains on the Cu(111) surface (Figure S8). Third, the cracks tended to propagate parallel to the grain boundary between the Cu(100) and (111) faces, as indicated by the arrows in Figure 5a. This anisotropic crack propagation was clearly confirmed by the distribution of the angles of the macroscopic crack direction with respect to the grain boundary (Figure 5b). These results indicate that the cracks were formed as a result of the stress concentrations at the V-shaped notches together with the uniaxial tension.

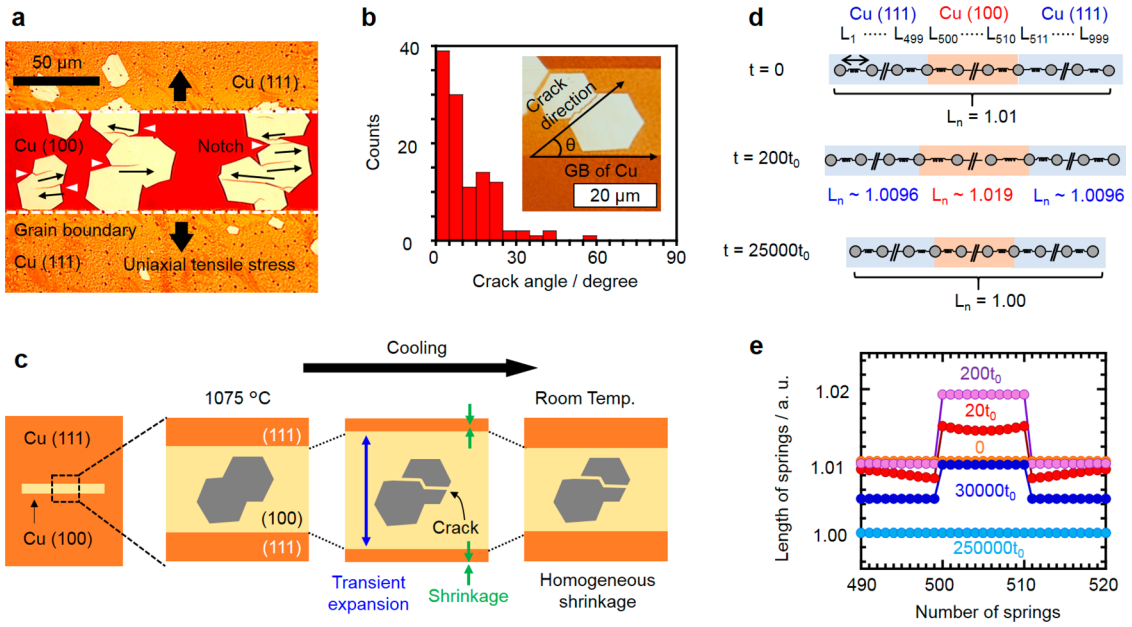

Figure 5. (a) Optical image of graphene grains on an oxidized Cu(100) face surrounded by Cu(111) faces. The red area corresponds to a Cu(100) face between orange Cu(111) faces. The face-dependent colors are likely derived from the difference in chemical reactivity between the (100) and (111) faces. (b) Distribution of the crack direction angle with respect to the grain boundary between the Cu(100) and (111) faces. (c) Schematic illustration of the formation mechanism of anisotropic cracks in graphene grains grown at 1075 °C on narrow Cu(100) faces by transient lattice expansion of narrow Cu(100) grains during the cooling. (d) Schematic cross-sectional illustration of the simulation model used for thermal shrinkage and its time evolution (t = 0, 200t_0 and 250 000t_0). The model consists of linearly distributed particles connected with springs and having free ends. The spring constants were set to 1, except for the central region (from the 500th to the 510th particle), corresponding to the narrow Cu(100) grain between the Cu(111) grains. The spring constants of this middle region were set to 0.5. Here, t_0 is defined as the inverse of the eigenfrequency of the outside springs. (e) Time evolution of the lengths of each spring from the 490th to the 520th particle.

When we considering the results above, the selective cracking in the zigzag direction is in good agreement with previous reports concerning MD simulations of the fracture of graphene under in-plane tension.[22,24] In this simulation, zigzag edges preferentially form from notches in the graphene regardless of the direction of the applied stress. This is interpreted to derive from the lower surface energy of zigzag edges, and the present result could support these simulation results. Unlike the previous tearing of graphene transferred onto a TEM grid,[16] the present cracking occurs in as-grown, clean graphene as the result of uniaxial tension. This could be a major factor in terms of realizing the crystallography-selective cracking of graphene.

When working toward controlling crack formation, it is important to understand the origin of the uniaxial tension. In the present study, graphene was grown at a high temperature (1075 °C) and then immediately cooled at a rate of 100−200 °C/s by taking the samples out of the furnace. Because Cu has a much larger thermal expansion coefficient than graphene,[33,34] we can expect that the thermal shrinkage of the Cu foil during this cooling will generate an overwhelming compressive lattice strain in the graphene. In fact, at room temperature, this compressive strain was confirmed by the upshift observed in the G- and 2D-bands in the Raman spectra of graphene on Cu foil (Figure S9), as has also been reported in previous Raman studies.[35,36] These findings strongly suggest that the uniaxial tension is applied in a transient manner to the graphene during the cooling step. As illustrated in Figure 5c, at the intermediate stage in the cooling process, the lattice expansion of a narrow Cu(100) grain could be accompanied by the thermal shrinkage of adjacent Cu(111). Such transient lattice expansion of Cu(100) grains transmits uniaxial tension to the graphene, resulting in the crack formation. At room temperature, all the Cu grains uniformly shrink and compressive stress is applied to graphene films.

To explain this transient tension, the thermal shrinkage of Cu was simulated using a simplified model of a one-dimensional lattice, by solving the classical Newtonian equation described in the Methods section. Figure 5d summarizes the model used in this simulation and its time evolution obtained from the results of numerical calculations. Importantly, this model predicts the transient expansion of springs along the central region corresponding to the narrow Cu(100) grains at an earlier stage (for example, t = 20t_0 and 200t_0 in Figure 5e). This transient expansion occurs due to the characteristic time difference between the inner and outer springs. We note that, after a sufficiently long time (t = 250 000t_0 in Figure 5e), the lengths of all springs have been reduced to 1.00 by dissipation. This shrinkage could induce compressive stress in the graphene, which is consistent with the upshift seen in

the G- and 2D-bands in the Raman spectra of graphene on Cu foil at room temperature (Figure S9). On the basis of the results of these numerical simulations, we propose that the transient lattice expansion of narrow Cu(100) grains transmits uniaxial tension to the graphene. The controlled introduction of such uniaxial tension could, therefore, provide an effective means of creating long, atomically smooth zigzag graphene edges through crack formation.

CONCLUSION

We have reported the cracking of graphene along a specific crystallographic orientation to generate zigzag edges. This selective cracking is consistent with the results of previous MD simulations concerning the fracture of graphene under uniaxial tension. Raman spectroscopy provides further evidence that the crack-derived edges have smoother zigzag edges than the chemically formed grain edges of CVD graphene. Using the graphene cracks, we have demonstrated the modulation of source−drain current by applying a gate voltage across the crack. Optical microscope observations indicated that local uniaxial tension is applied to the graphene notches during the cooling process. The results of numerical simulations suggested that the thermal shrinkage of adjacent Cu grains leads to the transient lattice expansion of narrow Cu(100) films, transmitting uniaxial tension to the graphene. The present results demonstrate the unique fracture characteristics of graphene films and provide a novel way to prepare clean, smooth zigzag edges. Such high-quality edges offer an ideal system for the study of the unique electric and magnetic properties of the edge state in graphene. In addition, we note that clean, smooth edges are useful as a substrate for one-dimensional heteroepitaxy to grow atomic layers of other materials, including hexagonal boron nitride (hBN).[37−39] Furthermore, the present approach using uniaxial tension can be applied to the structural control of edges in other two-dimensional materials such as hBN and transition metal dichalcogenides.

METHODS

Graphene was grown from methane on Cu foil (thickness: 20 μm, Nilaco) using the chemical vapor deposition method. The Cu foil was first annealed for 60 min in a quartz vessel under a mixture of argon (388 sccm) and hydrogen (12 sccm) at 1075 °C. Graphene was subsequently grown on the foil under a mixture of methane (15 ppm), hydrogen (6 sccm), and argon (179 sccm). The sample was then immediately removed from the furnace and allowed to cool to room temperature.

Optical images were captured using an optical microscope (Nikon, Eclipse-LV100D). Spatially resolved LEED patterns of graphene on Cu foil were obtained with a low-energy electron microscope with aberration correction (ACSPELEEM, Elmitec GmbH).[40] Raman spectra were acquired using a micro-Raman spectroscope (Renishaw, inVia) with an excitation laser operating at 532 nm. Prior to measurements, the graphene was transferred to SiO_2/Si substrates using a polymeric support. Graphene on Cu foil was spin-coated with poly(methyl methacrylate) dissolved in chlorobenzene (0.5%, 20 μL), after which the Cu foil was etched using an iron nitrate solution. The polymer-coated graphene films were placed on the SiO_2/Si substrates (SiO_2 layer thickness = 285 nm) and dried in air. The polymer was then removed by dissolving with acetone. Topographical images of samples were obtained using atomic force microscopy (Shimadzu, SPM-9600) in the tapping mode. To fabricate graphene-based FETs, Cr (5 nm) and Au (50 nm) were deposited on the graphene on SiO_2/Si substrates with a shadow mask. Unnecessary parts of the graphene were removed by scratching with a tungsten tip and etching with laser irradiation. Electrical measurements of the FETs were performed with a semiconducting device analyzer (Keithley, 4200-SCS) at room temperature under vacuum (10^{-2} Pa).

In the numerical simulations, the model consisted of linearly distributed particles connected with springs and having free ends. The number of particles was 1000, and each particle had the same mass. The spring constants were set to 1, except for the central region (from the 500th to the 510th particle) corresponding to the narrow Cu(100) grain between the Cu(111) grains. The spring constants of this region were set to 0.5 because of the difference in elastic properties between the thin films with Cu(100) and (111) faces.[41] In the simulation, the normalized natural lengths of each spring, L_0, were initially set to 1.01 in an equilibrium state at a high temperature. At a given time (t = 0), L_0 was changed to 1.00, corresponding to instantaneous cooling to room temperature in real systems. The 1% reduction in the value of L_0 was selected to be consistent with the thermal shrinkage of Cu from 1000 °C to room temperature.[33] Each spring was then allowed to contract or expand until the length of each of the springs reached exactly 1.00. The length of each spring was calculated by solving the classical Newtonian equation with dissipation:

$$m\frac{dv_i}{dt} = -k_i\Delta x_i + k_{i+1}\Delta x_{i+1} - \zeta v_i$$

where m, v_i, k_i, and ζ are the mass and velocity of the ith particle, the spring constant of the ith spring, and the dissipation constant, respectively. In addition, $\Delta x_i = x_{i+1} - x_i - L_0$, where x_i and l_i are the coordinate and the natural length of the ith spring, respectively. In these calculations, the value of ζ was set to 1.

Conflict of Interest: The authors declare no competing financial interest.

Acknowledgment. This work was supported by a Grant-in-Aid for Young Scientists (A) (No. 15H05412) and a Grant-in-Aid for Scientific Research on Innovative Areas (No. 26107530) from the Ministry of Education, Culture, Sports, Science and Technology (MEXT), Japan, and by the Izumi Science and Technology Foundation. M.F. thanks the Japan Society for the Promotion of Science (JSPS) for a Grant-in-Aid for JSPS Fellows and also acknowledges support from the IGER program. The authors also thank Y. Chiba (JX Nippon Mining & Metals) for conducting EBSD measurements.

Supporting Information Available: The Supporting Information is available free of charge on the ACS Publications website at DOI: 10.1021/acsnano.5b03079.

Additional figures as described in text (PDF)

REFERENCES AND NOTES

1. Novoselov, K. S.; Geim, A. K.; Morozov, S. V.; Jiang, D.; Zhang, Y.; Dubonos, S. V.; Grigorieva, I. V.; Firsov, A. A. Electric Field Effect in Atomically Thin Carbon Films. *Science* **2004**, *306*, 666–669.
2. Novoselov, K. S.; Jiang, D.; Schedin, F.; Booth, T. J.; Khotkevich, V. V.; Morozov, S. V.; Geim, A. K. Two-Dimensional Atomic Crystals. *Proc. Natl. Acad. Sci. U. S. A.* **2005**, *102*, 10451–10453.

3. Zhang, Y.; Tan, Y. W.; Stormer, H. L.; Kim, P. Experimental Observation of the Quantum Hall Effect and Berry's Phase in Graphene. *Nature* **2005**, *438*, 201–204.
4. Meyer, J. C.; Geim, A. K.; Katsnelson, M. I.; Novoselov, K. S.; Booth, T. J.; Roth, S. The Structure of Suspended Graphene Sheets. *Nature* **2007**, *446*, 60–63.
5. Geim, A. K.; Novoselov, K. S. The Rise of Graphene. *Nat. Mater.* **2007**, *6*, 183–191.
6. Nakada, K.; Fujita, M.; Dresselhaus, G.; Dresselhaus, M. Edge State in Graphene Ribbons: Nanometer Size Effect and Edge Shape Dependence. *Phys. Rev. B: Condens. Matter Mater. Phys.* **1996**, *54*, 17954–17961.
7. Son, Y. W.; Cohen, M. L.; Louie, S. G. Half-Metallic Graphene Nanoribbons. *Nature* **2006**, *444*, 347–349.
8. Kobayashi, Y.; Fukui, K.; Enoki, T.; Kusakabe, K.; Kaburagi, Y. Observation of Zigzag and Armchair Edges of Graphite Using Scanning Tunneling Microscopy and Spectroscopy. *Phys. Rev. B: Condens. Matter Mater. Phys.* **2005**, *71*, 193406.
9. Suenaga, K.; Koshino, M. Atom-by-Atom Spectroscopy at Graphene Edge. *Nature* **2010**, *468*, 1088–1090.
10. Girit, Ç. Ö.; Meyer, J. C.; Erni, R.; Rossell, M. D.; Kisielowski, C.; Yang, L.; Park, C.-H.; Crommie, M. F.; Cohen, M. L.; Louie, S. G.; et al. Graphene at the Edge: Stability and Dynamics. *Science* **2009**, *323*, 1705–1708.
11. Yang, R.; Zhang, L.; Wang, Y.; Shi, Z.; Shi, D.; Gao, H.; Wang, E.; Zhang, G. An Anisotropic Etching Effect in the Graphene Basal Plane. *Adv. Mater.* **2010**, *22*, 4014–4019.
12. Shi, Z.; Yang, R.; Zhang, L.; Wang, Y.; Liu, D.; Shi, D.; Wang, E.; Zhang, G. Patterning Graphene with Zigzag Edges by Self-Aligned Anisotropic Etching. *Adv. Mater.* **2011**, *23*, 3061–3065.
13. Han, M. Y.; Brant, J. C.; Kim, P. Electron Transport in Disordered Graphene Nanoribbons. *Phys. Rev. Lett.* **2010**, *104*, 056801.
14. Ci, L.; Xu, Z.; Wang, L.; Gao, W.; Ding, F.; Kelly, K.; Yakobson, B.; Ajayan, P. Controlled Nanocutting of Graphene. *Nano Res.* **2008**, *1*, 116–122.
15. Datta, S. S.; Strachan, D. R.; Khamis, S. M.; Johnson, A. T. Crystallographic Etching of Few-Layer Graphene. *Nano Lett.* **2008**, *8*, 1912–1915.
16. Kim, K.; Coh, S.; Kisielowski, C.; Crommie, M. F.; Louie, S. G.; Cohen, M. L.; Zettl, A. Atomically Perfect Torn Graphene Edges and Their Reversible Reconstruction. *Nat. Commun.* **2013**, *4*, 2723.
17. Cong, C.; Li, K.; Zhang, X. X.; Yu, T. Visualization of Arrangements of Carbon Atoms in Graphene Layers by Raman Mapping and Atomic-Resolution TEM. *Sci. Rep.* **2013**, *3*, 1195.
18. Kim, K.; Artyukhov, V. I.; Regan, W.; Liu, Y.; Crommie, M. F.; Yakobson, B. I.; Zettl, A. Ripping Graphene: Preferred Directions. *Nano Lett.* **2012**, *12*, 293–297.
19. Jia, X.; Hofmann, M.; Meunier, V.; Sumpter, B. G.; Campos-Delgado, J.; Romo-Herrera, J. M.; Son, H.; Hsieh, Y. P.; Reina, A.; Kong, J.; et al. Controlled Formation of Sharp Zigzag and Armchair Edges in Graphitic Nanoribbons. *Science* **2009**, *323*, 1701–1705.
20. Li, X.; Wang, X.; Zhang, L.; Lee, S.; Dai, H. Chemically Derived, Ultrasmooth Graphene Nanoribbon Semiconductors. *Science* **2008**, *319*, 1229–1232.
21. Cai, J.; Ruffieux, P.; Jaafar, R.; Bieri, M.; Braun, T.; Blankenburg, S.; Muoth, M.; Seitsonen, A. P.; Saleh, M.; Feng, X.; et al. Atomically Precise Bottom-up Fabrication of Graphene Nanoribbons. *Nature* **2010**, *466*, 470–473.
22. Zhang, B.; Mei, L.; Xiao, H. Nanofracture in Graphene under Complex Mechanical Stresses. *Appl. Phys. Lett.* **2012**, *101*, 121915.
23. Kawai, T.; Okada, S.; Miyamoto, Y.; Hiura, H. Self-Redirection of Tearing Edges in Graphene: Tight-Binding Molecular Dynamics Simulations. *Phys. Rev. B: Condens. Matter Mater. Phys.* **2009**, *80*, 033401.
24. Yin, H.; Qi, H. J.; Fan, F.; Zhu, T.; Wang, B.; Wei, Y. Griffith Criterion for Brittle Fracture in Graphene. *Nano Lett.* **2015**, *15*, 1918–1924.
25. Jia, C.; Jiang, J.; Gan, L.; Guo, X. Direct Optical Characterization of Graphene Growth and Domains on Growth Substrates. *Sci. Rep.* **2012**, *2*, 707.
26. Yu, Q.; Jauregui, L. A.; Wu, W.; Colby, R.; Tian, J.; Su, Z.; Cao, H.; Liu, Z.; Pandey, D.; Wei, D.; et al. Control and Characterization of Individual Grains and Grain Boundaries in Graphene Grown by Chemical Vapour Deposition. *Nat. Mater.* **2011**, *10*, 443–449.
27. Ogawa, Y.; Komatsu, K.; Kawahara, K.; Tsuji, M.; Tsukagoshi, K.; Ago, H. Structure and Transport Properties of the Interface between CVD-Grown Graphene Domains. *Nanoscale* **2014**, *6*, 7288–7294.
28. Lee, G.-H.; Cooper, R. C.; An, S. J.; Lee, S.; van der Zande, A.; Petrone, N.; Hammerberg, A. G.; Lee, C.; Crawford, B.; Oliver, W.; et al. High-Strength Chemical-Vapor–Deposited Graphene and Grain Boundaries. *Science* **2013**, *340*, 1073–1076.
29. Wei, Y.; Wu, J.; Yin, H.; Shi, X.; Yang, R.; Dresselhaus, M. The Nature of Strength Enhancement and Weakening by Pentagon–Heptagon Defects in Graphene. *Nat. Mater.* **2012**, *11*, 759–763.
30. Wu, J.; Wei, Y. Grain Misorientation and Grain-Boundary Rotation Dependent Mechanical Properties in Polycrystalline Graphene. *J. Mech. Phys. Solids* **2013**, *61*, 1421–1432.
31. Cancado, L. G.; Pimenta, M. A.; Neves, B. R.; Dantas, M. S.; Jorio, A. Influence of the Atomic Structure on the Raman Spectra of Graphite Edges. *Phys. Rev. Lett.* **2004**, *93*, 247401.
32. You, Y.; Ni, Z.; Yu, T.; Shen, Z. Edge Chirality Determination of Graphene by Raman Spectroscopy. *Appl. Phys. Lett.* **2008**, *93*, 163112.
33. Nix, F. C.; MacNair, D. The Thermal Expansion of Pure Metals: Copper, Gold, Aluminum, Nickel, and Iron. *Phys. Rev.* **1941**, *60*, 597–605.
34. Yoon, D.; Son, Y. W.; Cheong, H. Negative Thermal Expansion Coefficient of Graphene Measured by Raman Spectroscopy. *Nano Lett.* **2011**, *11*, 3227–3231.
35. Ferralis, N.; Maboudian, R.; Carraro, C. Evidence of Structural Strain in Epitaxial Graphene Layers on 6H-SiC(0001). *Phys. Rev. Lett.* **2008**, *101*, 156801.
36. Lee, J. E.; Ahn, G.; Shim, J.; Lee, Y. S.; Ryu, S. Optical Separation of Mechanical Strain from Charge Doping in Graphene. *Nat. Commun.* **2012**, *3*, 1024.
37. Miyata, Y.; Maeda, E.; Kamon, K.; Kitaura, R.; Sasaki, Y.; Suzuki, S.; Shinohara, H. Fabrication and Characterization of Graphene/Hexagonal Boron Nitride Hybrid Sheets. *Appl. Phys. Express* **2012**, *5*, 085102.
38. Liu, L.; Park, J.; Siegel, D. A.; McCarty, K. F.; Clark, K. W.; Deng, W.; Basile, L.; Idrobo, J. C.; Li, A.-P.; Gu, G. Heteroepitaxial Growth of Two-Dimensional Hexagonal Boron Nitride Templated by Graphene Edges. *Science* **2014**, *343*, 163–167.
39. Han, G. H.; Rodríguez-Manzo, J. A.; Lee, C.-W.; Kybert, N. J.; Lerner, M. B.; Qi, Z. J.; Dattoli, E. N.; Rappe, A. M.; Drndic, M.; Johnson, A. T. C. Continuous Growth of Hexagonal Graphene and Boron Nitride in-Plane Heterostructures by Atmospheric Pressure Chemical Vapor Deposition. *ACS Nano* **2013**, *7*, 10129–10138.
40. Taniuchi, T.; Kotani, Y.; Shin, S. Ultrahigh-Spatial-Resolution Chemical and Magnetic Imaging by Laser-Based Photoemission Electron Microscopy. *Rev. Sci. Instrum.* **2015**, *86*, 023701.
41. Baker, S. P.; Kretschmann, A.; Arzt, E. Thermomechanical Behavior of Different Texture Components in Cu Thin Films. *Acta Mater.* **2001**, *49*, 2145–2160.